THE ASTRONOMICAL JOURNAL, 121:3138–3148, 2001 June

BARNARD'S MEROPE NEBULA REVISITED: NEW OBSERVATIONAL RESULTS

G. H. HERBIG AND THEODORE SIMON
Institute for Astronomy, University of Hawaii, 2680 Woodlawn Drive, Honolulu, HI 96822
Received 2000 November 10; accepted 2001 March 1

ABSTRACT

IC 349 is a small, fan-shaped reflection nebula located only 30″ from 23 Tau; its nucleus is, by a factor 15, the brightest area of the Pleiades nebulosity. We propose that IC 349 is a fragment of the Taurus-Auriga molecular cloud that has been encountered by the Pleiades in that cluster's southward motion and is being illuminated and shaped by the radiation field of 23 Tau. New *Hubble Space Telescope* multicolor imagery and the structure, colors, and surface brightness of IC 349 are discussed in terms of that hypothesis. What is known of the proper motion of the nebula, what can be inferred of the properties of the nebula from its color, and what is expected from radiation pressure theory appear to be compatible with this cloudlet-encounter hypothesis.

Key words: open clusters and associations: individual (Pleiades) — reflection nebulae

1. INTRODUCTION

It is now realized that the spectacular reflection nebulosity illuminated by the B-type members of the Pleiades star cluster is not a remnant of the material from which those stars formed some 100 Myr ago, but is the result of the cluster, in its southeastward movement, having passed into an unrelated dust concentration. CO maps of the region (Ungerechts & Thaddeus 1987; Fukui & Mizuno 1991) show that the minor molecular clouds near the cluster lie at the western edge of the Taurus-Auriga complex. The agreement in CO velocities supports the idea that it is in fact a peripheral fragment of the Tau-Aur clouds that the cluster has encountered.

The brightest portion of the Pleiades nebulosity is IC 349, Barnard's Merope nebula, which was discussed in some detail by Herbig (1996, hereafter H96). On conventional photographs, it is concealed in the overexposed image of the 4th magnitude 23 Tau (Merope), about 30″ distant. The structure of IC 349 is quite unlike that of the general nebulosity; it is triangular in outline, with a semistellar nucleus at the apex nearest 23 Tau and an axis of symmetry pointing approximately in that direction. It contains considerable internal detail even at modest angular resolution. Clearly, it owes its illumination to that star; as far as can now be discerned, the spectra of IC 349 and 23 Tau are identical.

Since H96, a considerable amount of new information has been obtained or has emerged, hence this second paper. That new material consists of high-resolution *BVI* imagery obtained with WFPC2 at the *Hubble Space Telescope* (*HST*), improved astrometry from *Hipparcos*, ground-based measurement of the proper motion of IC 349 by B. F. Jones, and an (unsuccessful) attempt to measure the CO radial velocity with the Caltech Submillimeter Observatory. We also comment on the radial velocity of IC 349 reported by Barentine & Esquerdo (1999).

2. *HST* IMAGERY

The *HST* images were taken with the WFPC2 in the course of a single orbit on 1999 September 19 through filters F439W (to match the passband of B_J, exposure 600 s), F555W (V_J, 300s), F814W (I_C, 200s), and F1042M (400 + 200 s). The roll angle was chosen so that IC 349 was central in the 35″ × 35″ field of the planetary camera (PC1), while the saturated image of 23 Tau fell in the wide-field camera, WF2. Only one diffraction spike of the star plus some scattered light intrudes upon the IC 349 frame. The "pipeline" images were processed with IRAF tasks to remove defective pixels and cosmic-ray hits.

To produce the false-color image shown as Figure 1, the *BVI* images were co-aligned by reference to four field stars detectable on the WF images and normalized to the count rates expected for Vega, which is defined as having a magnitude of 0.00 in each color on the *HST*'s "Vegamag system" and for which zero-point magnitudes are given by Baggett et al. (1997).

The resolution of the *HST* images is about a factor 8 better than that of the ground-based images discussed in H96, and as a consequence, the model of IC 349 proposed there must be modified. IC 349 contains much complex structure that, it now appears, did not emanate from the "nucleus." (In H96, an outflow from the nucleus was hypothesized to explain the opening angle of the fan.) In outline, IC 349 is shaped like an arrowhead, with the nucleus at the apex, pointing toward 23 Tau. It will be argued in § 3 that this is also very nearly the direction of motion of IC 349 with respect to the star cluster. The earlier low-resolution images showed the nebula to be outlined by several ribs, or veins, well resolved in Figure 1. They are now seen to be cirrus-like ridges, well defined on the "upstream" side toward 23 Tau but with tattered "downstream" edges. A number of thin plumes extend upstream. Fainter structure exists between the ridges, much of it in short arcs convex to the upstream direction. The nucleus is only the brightest and, presumably, the densest nodule in the leading upwind ridge. There is no indication on the 0.812 μm (I_C) or 1.04 μm images, where the bluish nebulosity would be suppressed relative to a red star, that a point source is imbedded in the nucleus, which, at this scale, is clearly elongated. Two of the other three ridges contain fainter condensations of the same kind.

We propose that IC 349 is the consequence of a small cloud, probably containing some internal structure before it approached 23 Tau, that has been compressed and, to some degree, dispersed during the encounter by either the radiation pressure or wind of 23 Tau. The details are laid out in §§ 3 and 4, where we assume the former because radiation

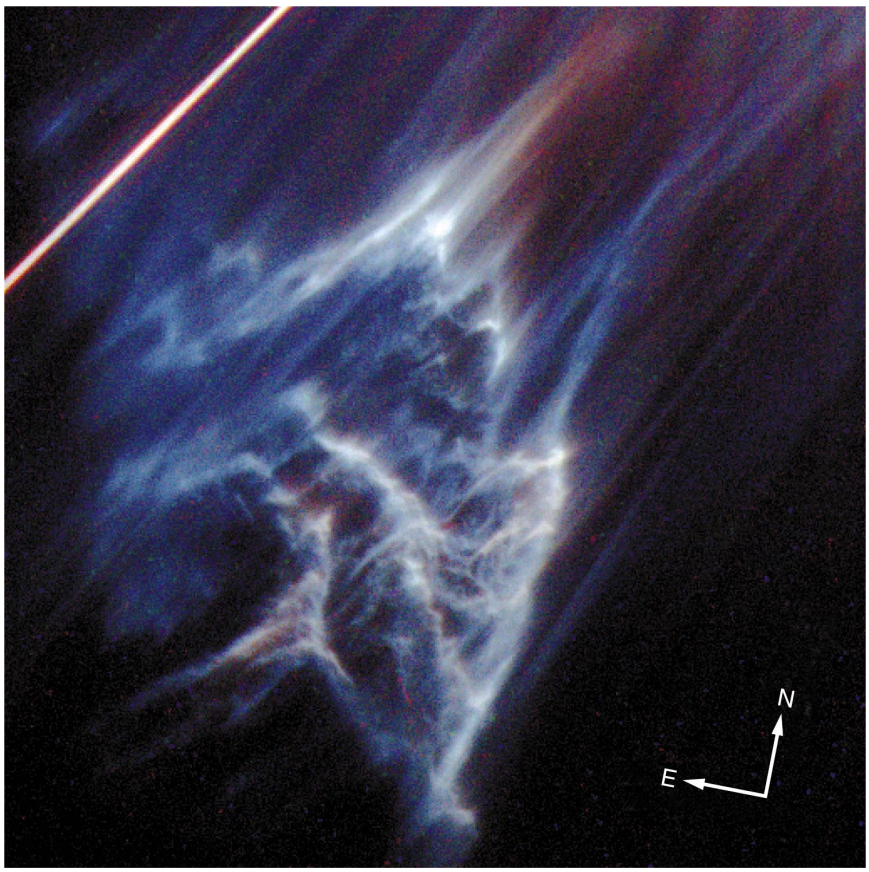

FIG. 1.—False-color representation of IC 349, constructed from the *HST BVI* images. Those frames were combined such that $B-V$ (and $V-I_C$) = 0 appears white, $B-V < 0.0$ blue, and $B-V > 0.0$ red.

pressure would have a demonstrably significant effect on IC 349, given the separation, the luminosity of 23 Tau, and plausible assumptions as to particle size and composition, while no significant stellar wind from the star has been reported.

We suppose that the composition of this cloudlet when it approached the Pleiades was typical of moderately dense interstellar clouds with respect to the relative abundances of H, CO, and solids. We assume the latter to be composed of silicates and graphite particles in comparable proportions, whose optical properties are those inferred from Mie theory.

2.1. *Photometry of the HST Images*

The aperture photometry of the *BVRI* images, based on the same zero points as above, employed an aperture radius of 11 pixels, equal to 0.″50. The background adopted was the median of measures at 64 points in the sky about 20″ west of IC 349. Table 1A gives the values of V, $B-V$, and $V-I_C$ at many locations over the surface of the nebula; their positions are shown on Figure 2. Within their uncertainties, this photometry is consistent with that of H96. Table 1B gives the same data for a number of points along the plume extending northward from the nucleus, between positions 1 and 36 in Figure 2, although to avoid clutter, their positions are not indicated there. The photometric errors listed in Tables 1A and 1B include the contribution of the scatter in the background.

Figure 3 was constructed to aid the eye in determining if there is a consistent pattern in the variation in color over the surface of IC 349. The coordinates X, Y are the $\Delta\alpha$, $\Delta\delta$ offsets of Tables 1A and 1B, following a 17° rotation, so that the positive Y-axis is directed toward 23 Tau. The direction of motion of the nucleus with respect to 23 Tau (see § 3) would be represented by a vector inclined 11° clockwise with respect to the vertical. The color at each of the points listed in Tables 1A and 1B is represented by a circle whose size increases as the colors become more *negative*. That is, $B-V$ values near 0.0 are shown as the smallest filled circles, and those near -0.5 as the largest. Similarly, $V-I_C$ values near $+0.1$ are the smallest open circles, while those near -0.9 are the largest. As will be discussed later, if differential radiation pressure has shaped IC 349, then a color gradient would be expected, in the sense that smaller particles and hence bluer colors would be farthest from the star, i.e., toward the bottom of the figure. Such a tendency is present on the left (northeast) side. Similarly, it is apparent on Figure 1 that the ridges and some of the minor structures in IC 349 have reddish fringes on their upstream sides.

2.2. *Theoretical Colors*

Not all particle sizes will be detectable in optical images, such as Figure 1. We assume that the particle size distribution of the original cloud has been preserved in IC 349 and is that inferred from the wavelength dependence of interstellar reddening by Mathis, Rumpl, & Nordsieck (1977 [hereafter MRN], but as modified by Draine & Lee 1984) for a mixture of silicate and graphite grains in proportion of 53:47. Figure 4 shows that function as a series of circles,

TABLE 1A

PHOTOMETRY OF STRUCTURE IN IC 349

No.	$\Delta\alpha$	$\Delta\delta$	V	$\epsilon(V)$	$B-V$	$\epsilon(B-V)$	$V-I_C$	$\epsilon(V-I_C)$
1	0.00	0.00	17.268	0.007	−0.125	0.013	−0.360	0.011
2	−2.17	−2.12	18.008	0.014	−0.114	0.025	−0.352	0.021
3	−2.42	−2.62	18.004	0.014	−0.148	0.024	−0.441	0.022
4	−4.55	−5.17	17.774	0.011	−0.051	0.021	−0.176	0.016
5	−4.67	−5.89	17.808	0.012	−0.069	0.022	−0.197	0.017
6	−4.63	−7.16	17.884	0.012	−0.052	0.023	−0.161	0.017
7	−4.48	−8.36	18.168	0.016	−0.124	0.029	−0.361	0.024
8	−4.42	−9.92	18.236	0.017	−0.143	0.030	−0.405	0.026
9	−3.91	−12.18	17.963	0.013	−0.137	0.023	−0.362	0.020
10.....	−3.72	−13.39	18.252	0.017	−0.145	0.030	−0.479	0.027
11.....	−3.64	−14.86	18.470	0.021	−0.139	0.037	−0.436	0.033
12.....	−3.02	−11.36	18.424	0.020	−0.129	0.036	−0.345	0.030
13.....	−1.63	−9.34	18.050	0.014	−0.107	0.026	−0.340	0.021
14.....	−1.40	−8.97	18.089	0.015	−0.102	0.027	−0.319	0.022
15.....	−0.56	−7.34	17.994	0.014	−0.151	0.024	−0.334	0.021
16.....	0.81	−6.44	17.869	0.012	−0.133	0.022	−0.320	0.018
17.....	3.63	−7.18	18.764	0.027	−0.312	0.043	−0.670	0.047
18.....	1.32	−8.48	18.343	0.019	−0.073	0.035	−0.145	0.025
19.....	1.11	−10.02	18.482	0.021	−0.142	0.037	−0.290	0.030
20.....	0.41	−11.86	18.801	0.028	−0.117	0.050	−0.294	0.040
21.....	2.34	−11.79	18.844	0.029	−0.092	0.054	−0.163	0.040
22.....	3.16	−12.68	19.554	0.056	−0.196	0.096	−0.405	0.084
23.....	4.39	−7.73	18.829	0.029	−0.335	0.046	−0.771	0.054
24.....	5.28	−8.31	18.749	0.027	−0.348	0.043	−0.791	0.051
25.....	6.59	−8.33	18.865	0.030	−0.352	0.047	−0.840	0.058
26.....	4.07	−10.98	19.942	0.081	−0.418	0.122	−0.881	0.160
27.....	0.37	1.22	17.848	0.012	−0.158	0.021	−0.341	0.018
28.....	1.49	−0.44	17.772	0.011	−0.179	0.019	−0.391	0.017
29.....	2.84	−2.05	18.119	0.015	−0.229	0.026	−0.492	0.024
30.....	4.49	−3.64	18.619	0.024	−0.365	0.038	−0.752	0.044
31.....	5.62	−4.60	18.760	0.027	−0.402	0.041	−0.828	0.052
32.....	6.72	−5.09	18.966	0.033	−0.451	0.049	−0.893	0.067
33.....	−4.57	−2.83	18.995	0.034	−0.312	0.054	−0.599	0.056
34.....	−4.93	−1.35	19.162	0.039	−0.377	0.060	−0.636	0.067
35.....	−5.89	2.84	19.454	0.051	−0.355	0.080	−0.208	0.070
36.....	−1.75	3.16	18.652	0.025	0.045	0.050	0.075	0.031
37.....	0.34	3.75	19.385	0.048	−0.250	0.080	−0.221	0.066

NOTES.—$\Delta\alpha$ and $\Delta\delta$ (in arcseconds) are measured with respect to the nucleus, at $3^h46^m20^s.06$, $+23°56'28''.4$ (J2000). For points 1–37, the magnitude and colors were measured with an aperture 1″.0 in diameter.

representing n, the number of particles per H atom in intervals 0.1 wide in $\log a$. (The filled circles show the range of a actually fitted by Mathis et al.; the open circles are an extrapolation.) The solid line is the (log) brightness in the V band expected for an optically thin, isotropically scattering, MRN mixture. It is proportional to $\pi a^2 Q_{\rm scat}\gamma n(a)d(\log a)$, where $Q_{\rm scat}$ is the scattering cross section, and γ is the albedo obtained for "smoothed astro-

TABLE 1B

PHOTOMETRY OF PLUME

No.	$\Delta\alpha$	$\Delta\delta$	V	$\epsilon(V)$	$B-V$	$\epsilon(B-V)$	$V-I_C$	$\epsilon(V-I_C)$
38.....	−1.78	3.26	21.300	0.013	0.045	0.051	0.129	0.038
39.....	−1.59	2.84	21.188	0.013	0.075	0.047	0.074	0.035
40.....	−1.39	2.51	21.092	0.012	0.058	0.043	−0.033	0.034
41.....	−1.19	2.14	20.992	0.012	0.025	0.039	−0.088	0.033
42.....	−0.98	1.81	20.884	0.011	−0.048	0.035	−0.159	0.032
43.....	−0.78	1.49	20.759	0.010	−0.063	0.031	−0.215	0.030
44.....	−0.58	1.11	20.578	0.010	−0.065	0.027	−0.282	0.027
45.....	−0.39	0.74	20.338	0.009	−0.125	0.022	−0.322	0.024
46.....	−0.20	0.37	19.749	0.007	−0.139	0.017	−0.302	0.018

NOTES.—These points lie on the plume extending between points 1 and 36 (Table 1A and Fig. 2). The data are as in Table 1A, except that for these points the aperture diameter was 0″.27.

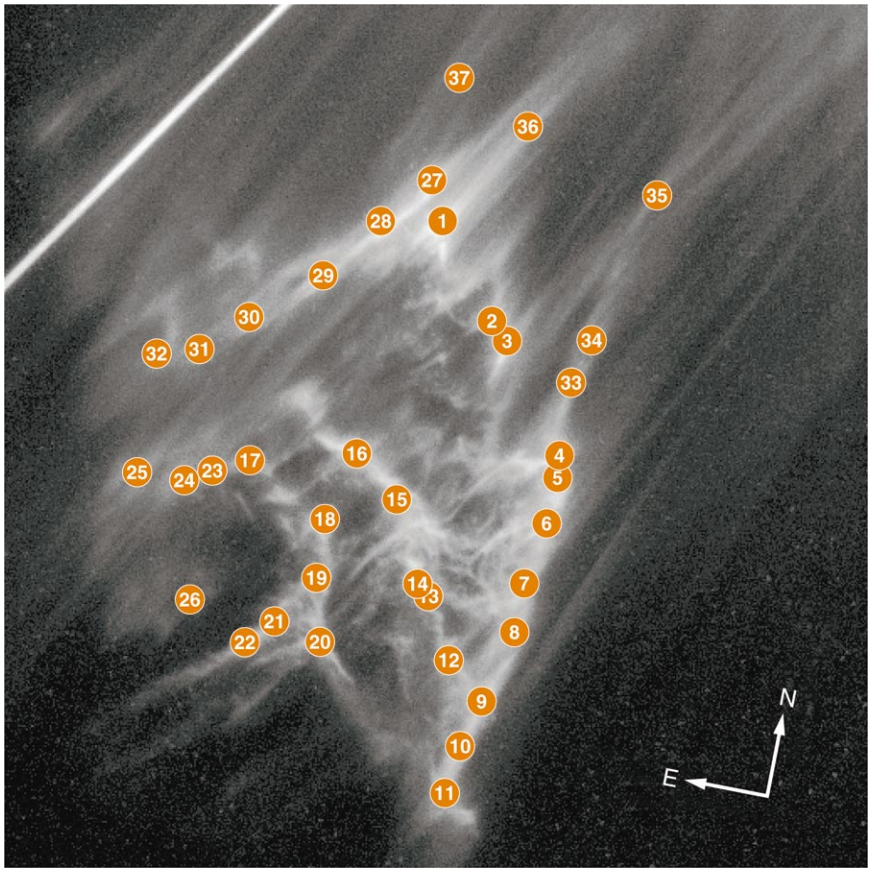

FIG. 2.—Location on the *HST* image of Fig. 1 of the points listed in Table 1A, which were measured for magnitude and colors. Table 1B contains the same information for points on the plume extending northward from the nucleus.

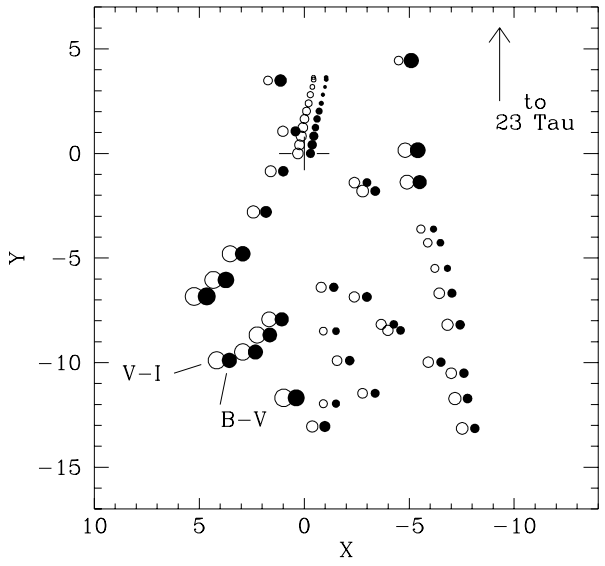

FIG. 3.—Variation of color over the surface of IC 349. The (X, Y)-coordinates correspond to the $\Delta\alpha$, $\Delta\delta$ offsets of Tables 1A and 1B, following a 17° rotation of the image, so that the positive Y-axis points to 23 Tau. The direction of motion (332°) would be represented by a vector inclined 11° clockwise to the vertical. The nucleus is at the origin, marked with a plus sign. Increasingly *negative* colors are represented by increasingly larger circles; the filled circles correspond to $B-V$, the open circles to $V-I_C$. The circles corresponding to the bluest and the reddest colors are identified specifically. There is a progression of increasingly bluer color with distance from the nucleus on the left side of the fan but not on the right.

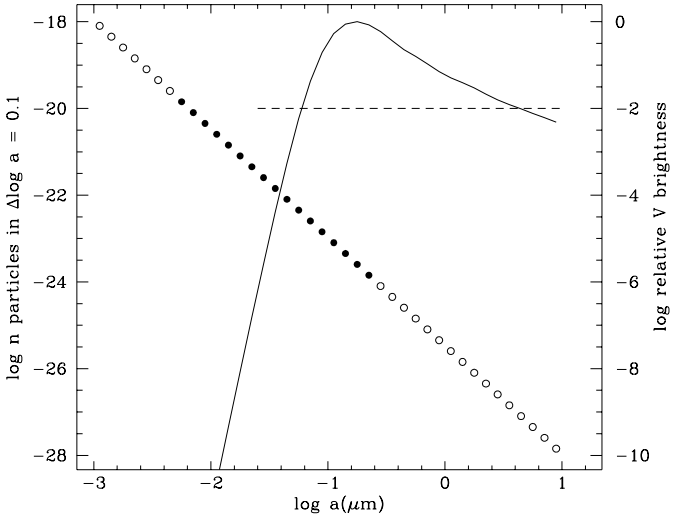

FIG. 4.—Circles (scale on the left) represent the power-law distribution of interstellar particle sizes from MRN, as modified by Draine & Lee (1984); n is the number of particles per H atom in an interval $d(\log a) = 0.1$ wide. The range of a actually fitted by MRN is indicated by filled circles; the open circles are extrapolated. The solid line (scale on the right) represents the (log of) expected brightness at $\lambda = 0.55$ μm contributed by $n(a)d(\log a)$ particles of radius a. The zero point is arbitrary. Given a population of particle sizes having the MRN distribution, one sees that particles of radii less than about 0.06 μm and greater than about 4 μm will contribute to the brightness of a scattering cloud at V less than 1% than do those at the $a = 0.2$ μm peak.

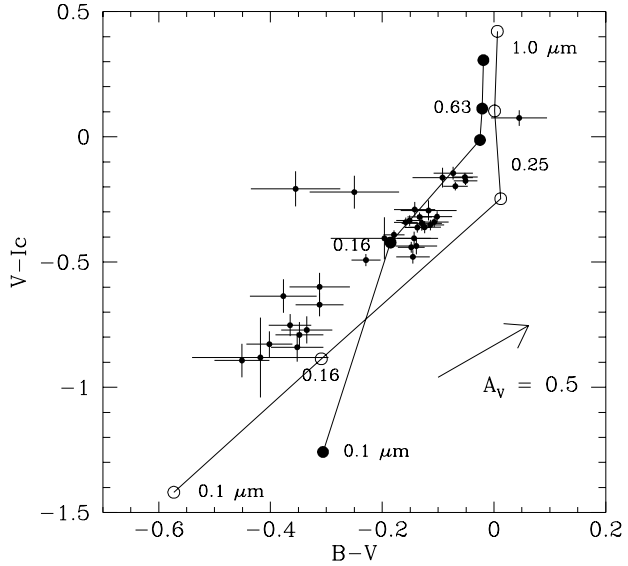

FIG. 5.—Small filled circles with error bars represent the $B-V$ and $V-I_C$ colors measured at the 37 points over the surface of IC 349 and listed in Table 1A. The large filled circles represent the theoretical colors of an optically thin cloud composed of an MRN mix of scatterers (0.53 silicate and 0.47 graphite, by number) and illuminated by a star of the observed colors of 23 Tau ($B-V = -0.06$, $V-I_C = +0.02$). The open circles represent the same for a 0.80:0.20 silicate and graphite mix. Particle radii are shown beside the circles. Here A_V (in eq. [1]) is set to 0.0.

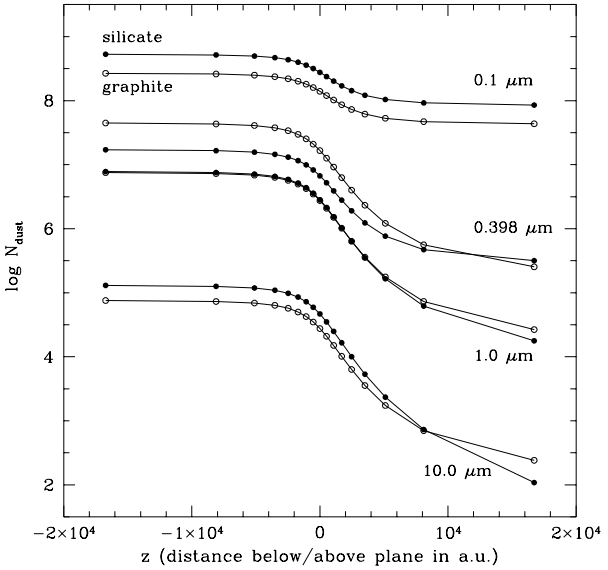

FIG. 6.—Column density of silicate and graphite particles of three different radii required to reproduce the V surface brightness of the nucleus of IC 349 for a range of distances of the nebula behind (negative z) or in front of the plane of the sky.

nomical silicate" and graphite at 25 K by interpolation in the tables from B. Draine;[1] the zero point is arbitrary. The curve peaks near $a = 0.2$ μm and falls below 1% of the peak at about 0.06 and 4 μm. On this basis and if the MRN distribution applies, then particles smaller and larger than those values will not contribute significantly to a V-band image.

The colors of an optically thin cloud of scatterers illuminated by 23 Tau follow from the optical properties of the particles. If the scattering is isotropic, the $B-V$ color is

$$(B-V)_{\rm neb} = (B-V)_* - 2.5 \log \left[\frac{(Q_{\rm scat}\,\gamma)_B}{(Q_{\rm scat}\,\gamma)_V}\right] + A_V(C_{BV} - 1)\,, \quad (1)$$

where the last term provides for the possibility of additional extinction either between the star and nebula or in the foreground of the nebula, in the amount A_V mag; $C_{BV} = A_B/A_V$. A similar expression holds for $V-I_C$. We approximate by taking $Q_{\rm scat}\gamma$ at the B and V mean wavelengths instead of a weighted average over the filter passbands. Figure 5 is a color-color plot based on the aperture data from Table 1A, shown as small filled circles with error bars. The series of connected filled circles represent the calculated colors for an optically thin cloud composed of an MRN mix of silicate (0.53 by number) and graphite (0.47) particles illuminated by a star having the observed colors of 23 Tau ($B-V = -0.06$, $V-I_C = +0.02$). The open circles show the same for a 0.80:0.20 mix of silicate to graphite. The particle radii range from $a = 0.1$ to 1 μm and are marked near each pair of circles.

One sees, to the extent of the assumptions implicit in Figure 5, that the range of colors in IC 349 can be accounted for by a spread in particle sizes by a factor of no more than about 5. Particles smaller than about $a = 0.1$ μm do not appear to be present; they would produce colors off the bottom left of that diagram. Consequently, we shall in what follows consider only particles having radii between 0.1 and 1.0 μm.

2.3. *How Much Dust?*

The column density of dust required to produce the observed surface brightness of the nucleus can be estimated in the following way. Consider a dust-filled cylinder of angular radius p and column density $N_{\rm dust}$, illuminated by 23 Tau of $V_* = 4.16$. According to H96, the total magnitude of the nucleus within $p = 1''.05$ is $V_n = 16.14$ (consistent with the present *HST* photometry), so $N_{\rm dust}$ is connected to the relative brightness of the star and 1 arcsec^2 of the nucleus as seen from Earth by

$$2.512^{V_*-V_n} = \gamma Q_{\rm scat}\, a^2 \phi(\alpha) \left(\frac{\sin^2\alpha}{4s^2}\right) \pi p^2 N_{\rm dust}\,, \quad (2)$$

while α is the scattering angle, a is particle radius, $\phi(\alpha)$ is the scattering phase function, and s is the projected separation of the nucleus and star; both s and p are in arcseconds. The Henyey-Greenstein phase function is adopted for both silicate and graphite particles.

The results depend hugely on particle radius and on the location of the scatterer along the line of sight. The plane of the sky is defined as that passing through 23 Tau. In a coordinate system to be used later, x and y lie in the plane of the sky, while z is normal to and positive in the direction of the Sun. Thus the sign of z, locating the scatterer in front of or behind the plane of the sky, controls α. The resulting values of log $N_{\rm dust}$ as a function of a and for $-1.7(4) \le z \le +1.7(4)$ AU are shown in Figure 6.[2] The average space density $n_{\rm dust}$ cm^{-3} of dust particles is about $N_{\rm dust}/3.7(15)$, the latter being the path length through the nucleus, assumed to be spherical.

[1] The tables are available at http://www.astro.princeton.edu/~draine. Those data were calculated by Draine from the theory of Laor & Draine (1993).

[2] We write $A(B)$ for $A \times 10^B$ throughout.

TABLE 2

DUST IN THE NUCLEUS OF IC 349

	SILICATE		GRAPHITE	
z (AU)	N_{dust} (cm^{-2})	A_V (mag)	N_{dust} (cm^{-2})	A_V (mag)
	$a = 10.0$ μm			
−20000.....	1.31 (5)	0.42	7.59 (4)	0.19
−10000.....	1.28 (5)	0.40	7.42 (4)	0.19
−5000	1.18 (5)	0.38	6.89 (4)	0.17
0	4.67 (4)	0.15	2.76 (4)	0.07
+5000	2.47 (3)	0.008	1.81 (3)	0.005
+10000.....	4.21 (2)	0.001	4.85 (2)	0.001
	$a = 1.0$ μm			
−20000.....	7.83 (6)	0.24	7.54 (6)	0.24
−10000.....	7.65 (6)	0.23	7.38 (6)	0.24
−5000	7.08 (6)	0.22	6.84 (6)	0.22
0	2.83 (6)	0.09	2.75 (6)	0.09
+5000	1.73 (5)	0.005	1.85 (5)	0.006
+10000.....	4.09 (4)	0.001	5.14 (4)	0.002
	$a = 0.1$ μm			
−20000.....	5.31 (8)	0.020	2.68 (8)	0.14
−10000.....	5.22 (8)	0.020	2.63 (8)	0.14
−5000	4.95 (8)	0.019	2.50 (8)	0.13
0	2.76 (8)	0.010	1.40 (8)	0.07
+5000	1.05 (8)	0.004	5.35 (7)	0.03
+10000.....	8.92 (7)	0.003	4.55 (7)	0.02

The dust extinction A_V, consequent upon these column densities, is $1.086 Q_{ext} N_{dust}$, where Q_{ext} is the total cross section for scattering plus absorption. It is given in Table 2, together with values of N_{dust} for both silicate and graphite particles at several representative values of z and for particle radii 1.0 and 0.1 μm, as well as for 10.0 μm, to illustrate the consequences at larger radii.

3. GEOMETRY OF THE ENCOUNTER

Our basic assumption, therefore, is that IC 349 is the result of the recent exposure to the radiation field of 23 Tau of what originally was a Tau-Aur cloudlet. We hypothesize that this subcloud, when it encountered the Pleiades, had the same space velocity vector as a present CO + T Tauri star concentration about 5° to the northeast, and that the geometry of the encounter can be constructed from a comparison of that vector with the same quantity for the Pleiades cluster.

The details are as follows: There is good evidence that young low-mass stars recently formed in a molecular cloud share the radial velocity of the cloud material (to within a few kilometers per second), so the proper motion of the cloud itself ought to be the same as that of the stars, measured astrometrically. The average radial velocity of the cloud is obtained from the molecular lines, so given the distance, the space motion of the cloud in some average sense is determinable. Specifically, a major concentration of T Tauri stars exists near 4^h14^m, +28° (B1950) near a peak in the Tau-Aur CO column density. The CO velocity at that point is known (Ungerechts & Thaddeus 1987, cloud 27C), while proper motions for some 17 of the stars involved have been measured by Jones & Herbig (1979). The distance of that concentration has been estimated from *Hipparcos* parallaxes as about 125 pc (Bertout, Robichon, & Arenou 1999), a value that we adopt, although the result is not sensitive to the choice. The resulting space velocity vector of that cloud is converted to proper motion and radial velocity at the position of the Pleiades (3^h44^m, +23°.9) and then compared with the same quantities for the Pleiades cluster. This is essentially the procedure followed by Olano & Pöppel (1987) and H96.

Since the latter investigations, however, *Hipparcos* parallaxes and proper motions on the FK5 system have become available for three of the 17 T Tauri stars (TTSs) discussed in H96 and for HD 283572 (B. F. Jones 1981, private communication, quoted by Walter et al. 1987). Proper motions for many of the same TTSs, also on the FK5 system, have been published by Frink et al. (1997). The Jones & Herbig (1979) proper motions were on a local system defined by a large number of faint—presumably background—stars, in regions of minimal obscuration on each plate. The correction to reduce these motions to the *Hipparcos* system, admittedly on the basis of only the four stars in common, is -2.5 ± 3.2 and -1.3 ± 2.8 mas yr^{-1}, so that the corrected mean proper motion for all 18 TTSs becomes $+4.3 \pm 3.5$ and -28.8 ± 3.0 mas yr^{-1}. The heliocentric radial velocity from CO is +15.8 km s^{-1}, which when transferred to the position of the Pleiades becomes +16.5 km s^{-1}. We accept the *Hipparcos* proper-motion, heliocentric radial velocity ($+5.7 \pm 0.5$ km s^{-1}) and distance (118 ± 3 pc) for the Pleiades from Robichon et al. (1999).

The resulting proper motion of IC 349 with respect to the Pleiades mean (which we assume to represent 23 Tau) is $\Delta\mu_\alpha \cos\delta = -9.5 \pm 3.5$, $\Delta\mu_\delta = +17.8 \pm 3.0$ mas yr^{-1}, or a cross motion of 11.3 km s^{-1} toward P.A. = 332°.

A direct measurement by B. F. Jones of the relative proper motion of the nucleus of IC 349 with respect to faint members of the Pleiades is quoted by Barentine & Esquerdo (1999): -15.2 ± 8.7 and $+15.4 \pm 15.2$ mas yr^{-1}. At 118 pc, this corresponds to 12.1 km s^{-1} toward 315°. These two vectors are displayed in Figure 7, which shows the total motions in 100 yr. The corresponding uncer-

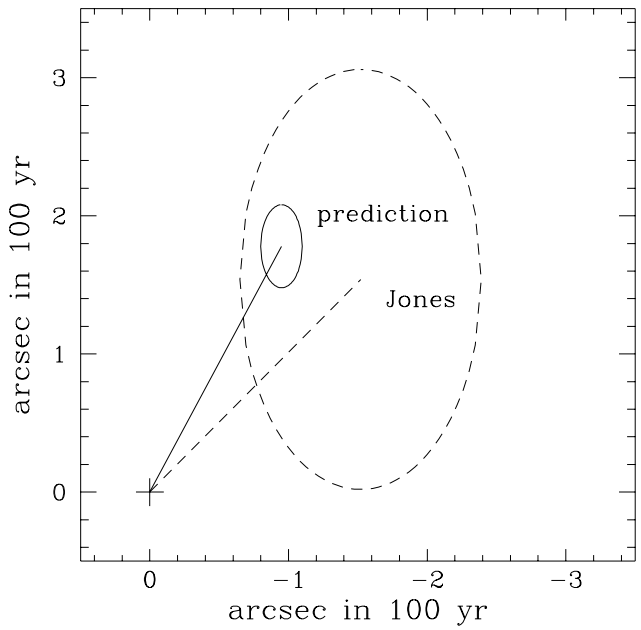

FIG. 7.—Expected error ellipse (*solid line*) in the x-y plane of the proper motion of the nucleus of IC 349 if it is a Tau-Aur subcloud (§ 3) and the error ellipse corresponding to the measures by B. F. Jones (*dotted line*).

tainties are represented as error ellipses. The two are in reasonable conformity; a consequence of this agreement is discussed below.

4. MOTION OF DUST IN THE GRAVITATIONAL AND RADIATION FIELD OF 23 TAURI

The trajectories of particles in a small optically thin cloud approaching 23 Tau have been computed as in H96, taking into account the gravitation and radiation pressure of the star, neglecting any braking due to interaction with any ambient cluster gas. The coordinate system is as projected upon the plane of the sky: the origin is at 23 Tau, x positive to the east, y positive to the north, z positive toward the Sun. The equation of motion in x is

$$\ddot{x} = \frac{-GM_*}{d^2}\frac{x}{d}(1-R) - \frac{3n\mu m_{\rm H}\,\delta v_x\,|\delta v_x|}{4a\rho}\,, \qquad (3)$$

where d is the distance from the star, $M_* = 4.0\,M_\odot$, and R is the ratio of radiation pressure to gravity; similar expressions hold for y and z.

$$R = \frac{3I}{4ac\rho GM_*}\,, \qquad (4)$$

where a is particle radius, ρ is particle density (assumed to be 3.3 for silicate and 2.26 g cm^{-3} for graphite), while c and G are the physical constants, and

$$I = \int_{0.05}^{10.0} Q_{\rm pr}(\lambda)F_*(\lambda)d\lambda\,. \qquad (5)$$

The second term in equation (3) expresses the drag exerted on the dust particle by the gas of the initial cloud, which is not affected by radiation pressure. The x-component of the velocity difference $v_{\rm dust} - v_{\rm gas}$ is δv_x, n is the gas density in atoms cm^{-3}, μ is the average molecular weight of the gas (taken to be 2.3), and $m_{\rm H}$ is the mass of a H atom. A factor that describes the angular distribution of the recoiling gas atoms is omitted.

In equation (5), $F_*(\lambda)$ is the flux of 23 Tau in ergs cm^{-2} s^{-1} μm^{-1}. The radiation field adopted for 23 Tau is a composite: from 0.05 to 1.0 μm, surface fluxes from a model atmosphere of $T_e = 14{,}500$, $\log g = 4.0$, solar metallicity (Kurucz 1979), converted to total fluxes with a radius of 3.5 $R_\odot$; *IUE* fluxes (Wu et al. 1983) for the B6 V star HR 4119 from 0.121 to 0.321 μm; scanner fluxes of HR 4119 by Wolff, Kuhi, & Hayes (1968) between 0.32 and 0.68 μm; and from 1.0 to 10.0 μm, a fit to the *JHKL* photometry of HR 4119 and 23 Tau by Johnson et al. (1966), by Gehrz, Hackwell, & Jones (1974), and by Dougherty, Taylor, & Clark (1991). These various series were adjusted to the distance of the Pleiades by allowance for the *Hipparcos* distance of HR 4119 and the reddening of 23 Tau, $E(B-V) = +0.09$. The values of $Q_{\rm pr}$, the efficiency factor for radiation pressure, were calculated from Draine's tables.

The luminosity of 23 Tau over this wavelength interval, by integration of the adopted $F_*(\lambda)$, is 509 $L_\odot$. Values of R for this radiation field, for a mass of 23 Tau of 4.0 $M_\odot$, and several particle radii are given in Table 3.

The numerical integration of equation (3) begins at a point on the backward track of the nucleus of IC 349, defined by its relative proper motion, at a time 5–10 $\times$ 10^3 yr before the present, when the gravitational and radiative influence of 23 Tau would have been negligible. The starting velocity at that time is that predicted by the Tau-Aur cloud scenario. At each time step, the coordinates, velocities, and accelerations are updated. Because dust and gas respond differently to radiation pressure, in the absence of gas drag on the dust, the two could become decoupled near the star.

TABLE 3

RATIO OF RADIATION PRESSURE TO GRAVITY FOR 23 TAURI

a (μm)	Silicate	Graphite
0.001	328.0	1086.0
0.00398.....	343.0	1110.0
0.01.....	436.0	1260.0
0.0398	583.0	1331.0
0.1	299.0	599.0
0.398	68.9	108.0
1.0	24.4	37.0
3.98.....	5.67	8.33
10.0.....	2.19	3.21

NOTES.—These values of R are specific to the assumed energy distribution and mass of 23 Tau.

4.1. *Motion in the Absence of Gas Drag*

If drag by the gas that accompanies the dust is ignored, the strong dependence of R on a means that radiation pressure will act to sift the dust according to particle size. Figure 8 is an illustration of this effect. It shows the trajectories of a cube, initially 400 AU on a side, composed of "astrosilicate" particles of radii 0.1, 0.398, and 1.0 μm. It

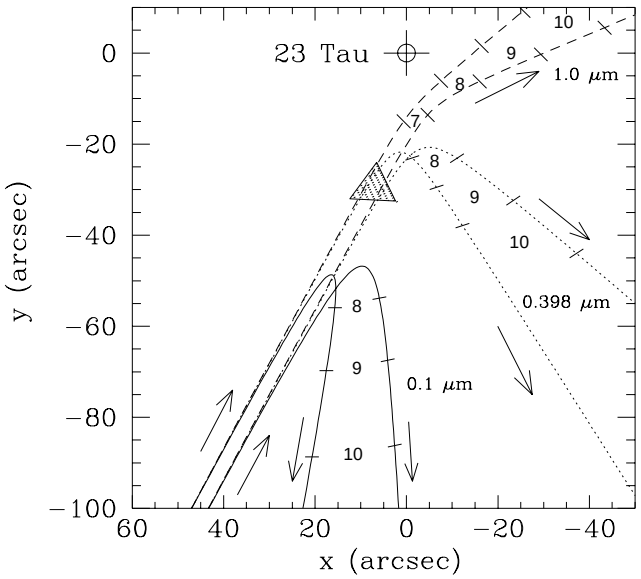

FIG. 8.—Paths of a cloud of silicate particles of three different sizes, initially well mixed, as they approach 23 Tau, moving toward P.A. 332°, with the velocity vector inferred for a Tau-Aur cloud. It is important to note that gas drag is not included. The projection is on the plane of the sky passing through 23 Tau. The initial configuration was a cube 400 AU on a side, and the curves show the subsequent envelope of that cube for the three particle sizes as they respond to the radiation pressure and gravitation of 23 Tau. The shaded triangle shows the present position of IC 349. The small numbers, 7, 8, etc., between the short lines on the curves indicate the position of each cube 7000, 8000, etc. yr after the calculation began.

approaches the present position of IC 349, moving toward P.A. 332°, with the cross motion and radial velocity derived in § 3 and a starting at $z_0 = 15{,}000$ AU. The shaded triangle indicates the present outline of IC 349 in this coordinate system, with 23 Tau at the origin. In equation (3), n is set to zero. One sees the sifting effect of radiation pressure in the dependence on particle size: the 0.1 μm particles turn around and are repelled well before reaching the present position of IC 349; those of 0.398 μm get somewhat nearer the star before being diverted and repelled, while the 1.0 μm particles are merely deflected. The tracks for graphite differ only in detail. Note that such calculations ignore the possibility that particle dimensions may change as they are warmed near the star.

Such calculations also demonstrate how a cloud approaching 23 Tau would be progressively flattened because of the differential effect of radiation pressure. As it approaches the "turnaround point," the front surface is compressed to the point that a shell is formed approximately at right angles to the direction of motion, as was noted by Arny (1977). To illustrate this effect, the three-dimensional cloud has been replaced by a linear array of $a = 0.398$ μm dust particles, originally 10″ long in projection, that has been allowed to approach the star directly. Figure 9 shows the evolution of its density profile. Just before the turnaround point, it is compressed by a factor of 5 in the direction of motion, and a density ratio of 5:1 has developed between the leading and following edges. This could explain the prominent ridge lines in IC 349, and the dependence of radiation pressure on particle size could account for the reddish upstream fringes on some of those ridges.

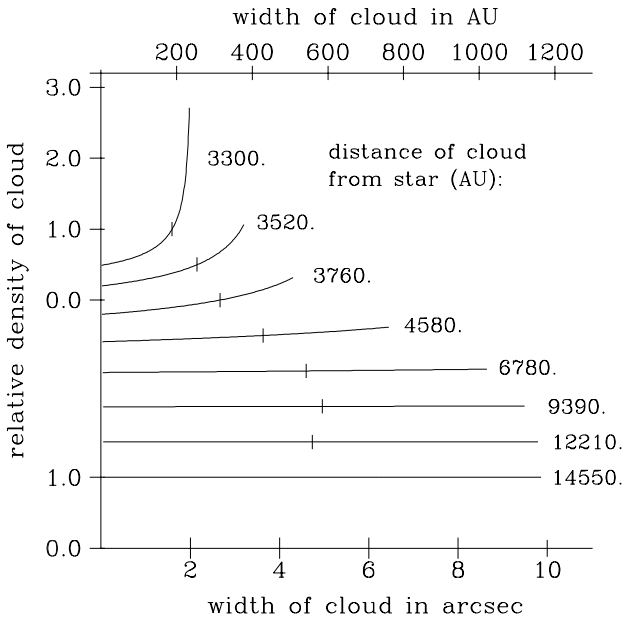

FIG. 9.—Evolution of the density profile of a one-dimensional array of $a = 0.398$ μm silicate particles as it approaches 23 Tau, in the absence of gas drag. The array at the starting point 1500 AU from the star was 10″ (=1180 AU) long with a flat density profile, represented by the horizontal line at the bottom. Time increases from bottom to top; as the array moves toward the star, it becomes compressed in the direction of motion, and the density on the leading edge begins to rise because of differential radiation pressure. The last profile corresponds to the present (projected) separation of IC 349 from the star, about 3300 AU. The array has been compressed by a factor of about 5, and the density on the leading edge has risen by about the same factor. The zeroes of the successive profiles are separated vertically by 0.5 for convenience of display. The abscissa origin of each profile is at the rearmost point of the array; the distance of that point from the star is shown on the right. The short lines mark the point on each profile at which the density has the starting value of 1.0.

There are two observational constraints on such calculations: (1) If the cloudlet was decelerating as it approached the turnaround point, its cross motion, would fall below the initial value of 11.3 km s^{-1}. The only information available on cross motion is Jones's measurement of the proper motion of the nucleus, which corresponds to 12.1 ± 9.8 km s^{-1}. The uncertainties are large, but if the motion is truly nonzero (and the rough agreement of its direction with that expected for a Tau-Aur cloudlet hints that this may be so), it means that the nucleus has not yet reached the turnaround point. A strenuous effort to improve the proper motion in order to sharpen this constraint is recommended. (2) Direct images show no sign of a major particle size–dependent breakup of IC 349, as would be expected from the trajectories in Figure 8. There is a systematic change in color on the northeast side of the fan (§ 2.1) in the sense that those colors become more negative with increasing distance from the star, as would be expected from the dependence of R on particle size. However, this is a small effect compared with that anticipated from Figure 8, where no drag force was included.

4.2. *Gas Content of IC 349*

Nothing is known about the amount of gas in IC 349. None of the shock-excited emission lines that might have been expected from its supersonic passage through a gaseous medium travelling with the cluster has been found. The gas density, not at IC 349 but averaged over the line of sight, can be estimated in two different ways.

1. Savage et al. (1977) obtained H_2 column densities from *Copernicus* absorption spectroscopy of 20, 23, and η Tau. The 21 cm observations of the Pleiades by Gordon & Arny (1984) revealed a component at $+16$ km s^{-1} (their $V_{LSR} = +7$ km s^{-1} feature) that peaks in the region containing most of the bright reflection nebulosity. It is largely enclosed in a rectangular area of 50′ × 105′, centered near 17 Tau. If the depth in the line of sight of this region corresponds to 80′, then the total path length through this H I cloud is $t = 8.5(18)$ cm. If the appropriate path length is $t/2$, then Savage et al.'s $N(H_2)$ for 23 Tau gives $n(H_2) \approx 30$ cm^{-3} for that star.

The contribution of neutral H to the total gas density can be estimated by comparing the H I column densities (read from Gordon & Arny's Fig. 5*a*) for 20, 23, and η Tau with Savage et al.'s $N(H_2)$ values, allowing for the difference in path lengths. The ratios H I/H_2 for those stars are 1.5, 0.6, and 1.8, so the total volume density is about twice $n(H_2)$, thus $n \approx 60$ cm^{-3}.

2. A less direct estimate of n can be obtained by scaling from the observations by Federman & Willson (1984) of a dense cloud about 16′ south of 23 Tau, for which they obtained a total gas density of ~300–500 cm^{-3}. The reddened B star HD 23512 is seen through this cloud but somewhat off center. Its $E(B-V)$ is 0.36, compared with 0.09 for 23 Tau, so if total gas density scales as color excess, then the upper limit on n for 23 Tau would be 75–125 cm^{-3}.

Consider now whether the density inferred from gas drag considerations is indeed compatible with a gas density of about 100 cm^{-3}.

4.3. *Effect of Gas Drag*

It is possible to adjust the value of n in these calculations so that drag nullifies the differential radiation pressure, and there is only a small separation of $a = 0.1$–1 μm particles by the time the cloudlet has reached the present position of IC 349, and deceleration is still small. The color gradient on the left side of Figure 3 is understandable if a separation of the smallest from the largest particles of about 10″ has accumulated by the time the cloud has reached the present position of IC 349. Furthermore, it has already been shown that (see Fig. 5) the observed range in color can be explained by a particle size spread of about a factor of 5.

Given a permissible angular spread (here 10″) between particles of radii 0.1 and 1.0 μm by the time the cloudlet has reached the present position of IC 349, there is a critical n that depends on z_0, the distance in the line of sight above or behind the plane of the sky at which the integration begins. A lesser density would permit the nebula to be spread out by a greater amount before reaching its present position, while a larger one would allow it to survive relatively unscathed. Test runs show that if n is about 100 cm^{-3}, then z_0 would have to be either greater than about 21,000 AU (in which case $z = 7200$ AU) or less than about $-10{,}000$ AU ($z = -24{,}000$ AU). That is, IC 349 must now be well above or behind the plane of the sky. The deceleration in cross motion for 1.0 μm particles would, in either case, have accumulated to less than 1 km s^{-1}.

As a caution against taking such calculations too literally, it is to be remembered that two poorly conditioned input parameters control the predicted movement of the nucleus across the x-y plane and the consequences of its approach to 23 Tau. Clearly, the value of z_0 is critical, but the position angle of the approach is also important. Whether it is really about 332° as the calculations assume awaits more precise astrometry of the nucleus.

5. RADIAL VELOCITY OF IC 349

The components of the velocity vector of IC 349 with respect to 23 Tau have been taken to be those of a Tau-Aur cloudlet at the Pleiades. From them, an optical radial velocity of IC 349 is predictable given z, the present line-of-sight distance of the nebula from the plane of the sky. A velocity obtained from the displacement of the lines of 23 Tau, scattered by IC 349, will be the sum of $\dot{r}$ (the time rate of change of the distance from 23 Tau), the true line-of-sight radial velocity $v_\odot$, and the radial velocity of 23 Tau itself (because it defines the origin of the velocity coordinate system):

$$v_{\rm opt} = (x/r)v_x + (y/r)v_y + (z/r)v_z + v_\odot + v_* , \qquad (6)$$

where $r = (x^2 + y^2 + z^2)^{1/2}$. Table 4 contains in column (2) the predicted values of $v_{\rm opt}$ for a plausible range of z, given an initial $v_\odot = -v_z = 10.8$ and $v_* = +5.7$ km s^{-1}. (Note the sign convention is such that a negative v_z is a velocity of recession.) A prediction is also possible from Jones's proper motion for the nucleus of IC 349, but only of $v_{\rm opt} - v_\odot$, because in that case, $v_\odot$ is unknown. Those values are given in column (3) of Table 4.

In an effort to determine the radial velocity of IC 349 directly, J. R. Deane very kindly observed IC 349 for us in the ^{12}CO (2–1) line at the Caltech Submillimeter Observatory on Mauna Kea. The pointings alternated between the position of the object and a reference field at $3^{\rm h}45^{\rm m}30^{\rm s}$, $+24°15'0''$ (B1950) for a total of 130 minutes. The bandpass was 400 km s^{-1}, centered at $V_{\rm LSR} = 0.0$ km s^{-1}. However, no signal above the 3 σ noise level of 0.14 K km s^{-1} was detected.

TABLE 4

PREDICTED VALUES OF THE OPTICAL RADIAL VELOCITY OF IC 349

z (AU) (1)	Tau-Aur $v_{\rm opt}$ (km s^{-1}) (2)	Jones $v_{\rm opt} - v_\odot$ (km s^{-1}) (3)
−10000.....	+23.8	+2.7
−5000	+20.2	+0.4
−2000	+13.5	−3.0
−1000	+9.6	−4.3
0	+5.5	−4.8
+1000	+2.6	−4.3
+2000	+1.3	−3.0
+5000	+1.6	+0.4
+10000.....	+3.0	+2.7

The most promising spectral region for determining the optical radial velocity of IC 349, given the spectral type of 23 Tau and its large rotational broadening, is shortward of about 4500 Å. Thus the early Lick spectrograms of the red region are unsuitable. Arny's (1977) was the first attempt in the blue but at low resolution ($R \approx 3000$–6000). His velocity of +5 km s^{-1} was based on a single line; there was no estimate of its uncertainty. One notes, however, that this is within the range of possibilities listed in column (2) of Table 4.

The measurement of the velocity of IC 349 by Barentine & Esquerdo (1999) was made at $R = 27{,}000$ and included a careful check of their velocity system by observations of standard-velocity stars, following which they concluded that the velocity of the nucleus is -44.4 ± 5.4 km s^{-1}. The quality of their instrumentation and the care taken during the observations entitle this result to respect, but we see no way to reconcile it with the predictions in Table 4 or the scenario pursued in this paper, namely that IC 349 is a fragment of the Tau-Aur clouds. Barentine & Esquerdo reach the same conclusion, that on the basis of their velocity, "IC 349 is an interloper in the Pleiades," and it does not share the space motion of Tau-Aur cloud stars.

There is no obvious reason to discount this result, despite its conflict with our vision of IC 349. The idea of a rogue interstellar cloud bursting through the Pleiades cluster from behind is interesting but clearly deserves confirmation. One might expect that if such a cloud extended beyond the optical boundary of IC 349, some part might be projected upon 23 Tau and so produce a shortward-shifted interstellar absorption line. No such component has been reported in Na I, Ca II, or CH^+. (The 21 cm observations of Gordon & Arny [1984] do not extend to that velocity.) We believe it important to remeasure the radial velocity of IC 349 either optically or in CO or another molecular line.

6. DISCUSSION AND FINAL REMARKS

The dust and gas at IC 349 must be part of a much larger cloud in the foreground of the Pleiades cluster because all the brighter cluster members, whose interstellar Ca II and Na I lines have been studied by White (1984) and White et al. (2001), including 23 Tau, have their strongest component near +16.5 km s^{-1}, which is very near the velocity expected for a Tau-Aur cloud at that position. As noted in § 4.2, there

is also an extended H I cloud in this area having that same velocity. Individual stars differ in their subsidiary Na I structure; 23 Tau has a second, somewhat weaker component, at $+19$ km s^{-1}, which is the molecular line velocity of the Federman-Willson cloud south of 23 Tau and also of a secondary component in the 21 cm H I line. Several Pleiades stars are near enough to this extended cloud to illuminate dust in their immediate vicinity: 20 and 23 Tau, in particular, and 17 and η Tau to a lesser degree. However, the ^{12}CO survey of the region by J. Bally (private communication) shows minimal CO within the cluster, the main concentration being at the Federman-Willson cloud. That area, which is conspicuous in the 25, 60, and 100 μm *IRAS* maps (Castelaz, Sellgren, & Werner 1987) is faintly illuminated in blue light, probably by the integrated light of the cluster. The motion of the Pleiades will, in about 3 (4) years, bring 23 Tau very near the present location of this cloud.

IC 349 owes its high surface brightness to the accident of its proximity to 23 Tau. Do similar dust concentrations exist elsewhere in the $+16$ km s^{-1} cloud? The surface brightness of the nucleus of IC 349 is about 15 times greater than that of the next-brightest area in the general Pleiades reflection nebulosity, so it could be $15^{1/2}$ times farther from 23 Tau before becoming lost in the background. This defines a detectable radius around that star. Similar radii follow for 16, 17, 19, 20, and η Tau after scaling by their relative V magnitudes. The result is that the volume around 23 Tau comprises about 9% of the total in which such a nucleus would be detectable. We have imaged all five of these stars at the 2.2 m telescope, with the same setup used for 23 Tau in H96, but have found nothing resembling IC 349. We conclude it unlikely that "dark IC 349s" are numerous in that volume of the Pleiades.

The faint background of the extended Pleiades reflection nebulosity near 23 Tau appears as a series of nearly parallel striations. The position angles of most of these filaments range between 325° and 330°. The plumes that extend upstream from the arrowhead of IC 349 are near but not quite parallel to that structure; they scatter between about 334° and 339°. The similarity of both of these to the direction toward which IC 349 is moving with respect to 23 Tau (about 332° according to our hypothesis) is intriguing. The idea (suggested by Arny 1977) that these striations are simply Tau-Aur dust being carried through the cluster is attractive, but it does not explain why the filamentary structure around other Pleiades stars is aligned at quite different position angles. Whether the streakiness of this structure is caused by the proximity of the Pleiades stars or was inherent to the original cloud is unknown. We do note that 72 Tau, not a Pleiades member (it lies about 10° to the east) but at the edge of the main Tau-Aur clouds, illuminates a reflection nebulosity of its own that shows similar filamentary structure. It would be difficult to understand the complex appearance of IC 349 if the density distribution of the original dust cloud that approached 23 Tau had been smooth and structureless. What one sees in Figure 1 must be a result of the mutilation of original structure by radiation pressure.

Finally, our proposition is that the optical nebulosity IC 349 is the dust component of a small Tau-Aur cloudlet, imbedded in a larger gas envelope, that is passing near 23 Tau and, in the process, is being shaped by the radiation field of that star. A number of the observable properties of IC 349 are thereby understandable: (1) The Jones proper motion of IC 349 is uncertain, but in amount and direction, it is not in disagreement with expectation. (2) The optical interstellar lines produced by material in the foreground of 23 Tau are very nearly at the velocity expected, as is the velocity of one component in the 21 cm H I line. (3) The color variation across the southeastern surface of IC 349, with colors tending to become more negative with increasing projected distance from 23 Tau, is in the sense expected (because smaller particles are more repelled by radiation pressure than larger). (4) A spread by a factor of about 5 in the radii of particles (in the range 0.1 to about 1 μm) can explain this color variation. (5) The surface brightness of the nucleus can be reproduced by reasonable column densities of particles in that size range.

Our basic hypothesis does *not* account for the radial velocity of IC 349 reported by Barentine & Esquerdo (1999). We repeat that a redetermination of the optical radial velocity of IC 349 or a strong effort to detect it in a radio frequency molecular line is very desirable, the latter because it would give the radial velocity directly without the complication inherent in a velocity measured from the scattered stellar spectrum. Also important would be a precise determination of the proper motion, which ought to be possible since old photographic plates are known to exist in the Oxford, Lick, Allegheny, and perhaps other archives (references in H96).

Partial support for this work was provided by NASA through grant number GO-04510.02-92A from the Space Telescope Science Institute, which is operated by the Association of Universities for Research in Astronomy, Inc., under NASA contract NAS 5-26555. We are most indebted to Bruce Draine for making his calculations of the optical properties of "astrosilicate" and graphite available, to John Bally for access to his unpublished CO maps of the Pleiades, and to James Deane for his attempt to detect IC 349 in ^{12}CO (2–1). We are also grateful to Karen Teramura for preparing Figures 1 and 2.

REFERENCES

Arny, T. 1977, ApJ, 217, 83
Baggett, S., Casertano, S., Gonzaga, S., & Ritchie, C. 1997, Instrument Science Report WFPC2 97-10 (Baltimore: STSci)
Barentine, J. C., & Esquerdo, G. A. 1999, AJ, 117, 1402
Bertout, C., Robichon, N., & Arenou, F. 1999, A&A, 352, 574
Castelaz, M. W., Sellgren, K., & Werner, M. W. 1987, ApJ, 313, 853
Dougherty, S. M., Taylor, A. R., & Clark, T. A. 1991, AJ, 102, 1753
Draine, B. T., & Lee, H. M. 1984, ApJ, 285, 89
Federman, S. R., & Willson, R. F. 1984, ApJ, 283, 626
Frink, S., Röser, S., Neuhäuser, R., & Sterzik, M. F. 1997, A&A, 325, 613
Fukui, Y., & Mizuno, A. 1991, in IAU Symp. 147, Fragmentation of Molecular Clouds and Star Formation, ed. E. Falgarone, F. Boulanger, & G. Duvert (Dordrecht: Kluwer), 275
Gehrz, R. D., Hackwell, J. A., & Jones, T. W. 1974, ApJ, 191, 675
Gordon, K. J., & Arny, T. T. 1984, AJ, 89, 672
Herbig, G. H. 1996, AJ, 111, 1241 (H96)
Johnson, H. L., Mitchell, R. I., Iriarte, B., & Wiśniewski, W. Z. 1966, Comm. Lunar Plan. Lab., 4, 99
Jones, B. F., & Herbig, G. H. 1979, AJ, 84, 1872
Kurucz, R. L. 1979, ApJS, 40, 1
Laor, A., & Draine, B. T. 1993, ApJ, 402, 441
Mathis, J. S., Rumpl, W., & Nordsieck, K. H. 1977, ApJ, 217, 425 (MRN)
Olano, C. A., & Pöppel, W. G. L. 1987, A&A, 179, 202
Robichon, N., Arenou, F., Mermilliod, J.-C., & Turon, C. 1999, A&A, 345, 471
Savage, B. D., Bohlin, R. C., Drake, J. F., & Budich, W. 1977, ApJ, 216, 291

Ungerechts, H., & Thaddeus, P. 1987, ApJS, 63, 645
Walter, F. M., et al. 1987, ApJ, 314, 297
White, R. E. 1984, ApJ, 284, 685
White, R. E., Allen, C. L., Forrester, W. B., Gonnella, A. M., & Young, K. L. 2001, ApJS, 132, 253
Wolff, S. C., Kuhi, L. V., & Hayes, D. 1968, ApJ, 152, 871
Wu, C.-C., et al. 1983, IUE Ultraviolet Spectral Atlas of Selected Astronomical Objects (Washington: NASA)